INTERNATIONAL JOURNAL OF HYDROGEN ENERGY XXX (2011) 1–10

Available online at www.sciencedirect.com

SciVerse ScienceDirect

journal homepage: www.elsevier.com/locate/he

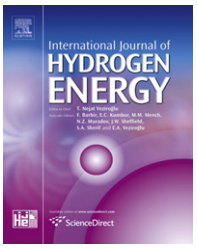

Structural and electrochemical characterization of $La_{2-x}Sr_xNiTiO_{6-\delta}$

J.C. Pérez-Flores [a,*], C. Ritter [b], D. Pérez-Coll [c], G.C. Mather [c], J. Canales-Vázquez [d], M. Gálvez-Sánchez [d], F. García-Alvarado [a], U. Amador [a]

[a] Universidad San Pablo CEU, Departamento de Química, Urb. Montepríncipe, Boadilla del Monte, E-28668 Madrid, Spain
[b] Institut Laue-Langevin, BP 156-38042 Grenoble, Cedex 9, France
[c] Instituto de Cerámica y Vidrio-CSIC Campus Cantoblanco, C/Kelsen 5, E-28049 Madrid, Spain
[d] Renewable Energy Institute, Castilla-La Mancha University; E- 02006-Albacete, Spain

ARTICLE INFO

Article history:
Received 1 September 2011
Received in revised form
24 October 2011
Accepted 28 October 2011
Available online xxx

Keywords:
SOFC
Thermal expansion
Compatibility
Double perovskite
Fuel cell cathode
Polarization

ABSTRACT

Materials of the series $La_{2-x}Sr_xNiTiO_{6-\delta}$ ($0 \leq x \leq 0.5$) have been characterized by both structural and electrochemical methods in order to assess their possible use as electrodes for SOFCs. Neutron and X-ray powder diffraction experiments have shown that they are stable under both oxidizing and reducing conditions while chemically compatible with YSZ at SOFC operating temperatures. Moreover, the thermal expansion has been determined to be isotropic with $\alpha_L = 10.0(3) \times 10^{-6}$ K^{-1}. This value is similar to that found for other perovskite materials used in SOFCs. However, polarization resistances reveal modest values of electrochemical response under oxygen (1.5 Ω cm^2 at 900 °C) and are quite poor in 5%H_2/N_2 mixtures (15 Ω cm^2) at the same temperature. Nevertheless, microstructure has not been optimized fully enough to discard the material as a potential SOFC cathode.

1. Introduction

The development of solid oxide fuel cells (SOFC) and their subsequent commercialization face several problems which are not yet fully solved satisfactorily. An SOFC is a complex ceramic device consisting of three main components, anode, electrolyte and cathode, all of which require extensive research of electrochemical properties, long-term stability and interfacial compatibility aspects in order to improve their performance. Several detailed review papers have been recently published dealing with the most relevant aspects of SOFC working conditions and materials [1–9]. Considering only material properties (processing and assembly present their own difficulties) a single cell specific resistivity of ca. 0.45 Ω cm^2 can be estimated as the upper limit for practical applications [1]. State-of-the-art SOFCs materials are far from rendering such performances (even at high temperatures); intense research is, therefore, needed to find innovative oxides to be used in commercial SOFCs.

In recent years, great efforts have been devoted to the development of intermediate temperature (IT) SOFC materials, which work in the temperature range 773–1073 K. Lowering the operating temperature has many advantages [1,5,9], although operation at low temperature requires significant improvements of the employed materials.

* *Corresponding author*. Tel.: +34 913510496; fax: +34 913724715.
E-mail address: jcaperez@ceu.es (J.C. Pérez-Flores).
0360-3199/$ – see front matter
doi:10.1016/j.ijhydene.2011.10.101

Perovskite-type compounds (ABO_3) have been extensively considered in the development of new materials which are potentially useful as electrodes in SOFCs, due to their ability to stabilize mixed metal oxidation states and high concentrations of oxygen vacancies. Aliovalent substitution on the A or B position may produce oxygen vacancies and hence an enhancement of ionic conductivity. On the other hand, when B is occupied by adequate suitable transition metal, mixed oxidation states can be stabilized at different oxygen partial pressures, changing both the nature and magnitude of the electronic conductivity. Therefore, mixed ionic–electronic conductivity (MIECs) and high catalytic activity can be found [2,10,11]. However, these attractive possibilities in terms of SOFC materials chemistry are countered by several drawbacks including relatively weak mechanical strength [12] and poor chemical stability under reducing conditions at high temperatures [13].

The most representative perovskite used as cathode material is $La_{1-x}Sr_xMnO_{3-\delta}$ (LSM), which represents the state of the art in the operating range 700–900 °C. It displays high electrical conductivity, high thermal stability, and compatibility with most electrolytes (YSZ, GDC and LSGM) at operating conditions, as well as excellent microstructural and long-term performance stability [14,15]. By contrast, its reduced ionic conductivity, and hence poor electrocatalytic activity, restricts its use to high temperature applications in which it must form a composite with an ionic conductor [16–18]. Recent investigations have shown that the electrode reaction is more complicated than the commonly accepted mechanism, based on the triple phase boundary (TPB) model [19,20]. Sr-substituted cobaltites, $La_{1-x}Sr_xCoO_3$ (LSC), constitute an alternative to Mn-based cathode materials; they exhibit mixed ionic-electronic conductivity to yield an excellent cathode performance with exceptionally low overpotential [21]. However, cobaltites show a very high thermal expansion which leads to the failure of the interconnect with the electrolyte, and subsequent loss of performances after thermal cycling. Alternative materials under investigation show promise in overcoming all these difficulties. These include $La_{1-x}Sr_xFeO_3$ (LSF), $La_{1-x}Sr_xCo_{1-y}Fe_yO_3$ (LSCF), $La_{1-x}Ba_xCo_{1-yFey}O_3$ (LSBC), $Pr_{0.6}Sr_{0.4}(Co_{0.2}Fe_{0.8})_{1-x}Sc_xCo_{0.5}Fe_{0.5}O_3$ and other derived compositions [7,15,17,22–25].

The requirements for a suitable anode material have been clearly established [5,26]: (i) the compound must have adequate electronic conductivity in the reducing atmosphere at the anode; (ii) a high catalytic activity is required so that the material can accept electrons from H_2 or the hydrocarbon used as fuels; (iii) the ionic conductivity must be high enough to allow for oxygen ions to diffuse rapidly from the electrolyte to the surface of the anode. Furthermore, anodes must be compatible with the electrolyte. Presently, the Ni/YSZ cermet constitutes the state of the art in anode technologies, although ageing produces agglomeration of Ni grains, and coking occurs when hydrocarbons are used as fuel at low temperature and Ni has a low sulphur tolerance. This is the reason why many research groups are exploring new options. Perovskite compounds appear once again to be interesting candidates because of their compositional flexibility and chemical stability, solving some of the problems found in nickel-based anodes. For example, $La_{0.75}Sr_{0.25}Cr_{0.5}Mn_{0.5}O_3$ (LSCM) forms nickel-free electrodes while showing a comparable anode performance to Ni/YSZ [27,28], with conductivity values of 38 S/cm at an oxygen partial pressure of 10^{-10} atm, with *p*-type as the dominant conduction mechanism. Improved performances are also found for $La_{1-x}Sr_xCo_yTi_{1-y}O_{3-\delta}$, which behaves as a mixed ionic-electronic conductor with values of 63 S/cm and 6×10^{-3} S/cm for electronic and ionic conductivity, respectively, at 700 °C [29]. Not only the A-site deficient LSCM, $(La_{0.75}Sr_{0.25})_{0.9}Cr_{0.5}Mn_{0.5}O_{3-\delta}$, but also other related double perovskites, $(La,Sr)_2M_{1-x}Cr_{1+x}O_6$ with M = V, Mn, Fe, Co, Ni and Cu, have been studied as anodes, and shown to have improved performances [27].

The materials used as electrolyte in SOFC must be chemical and physically stable under reducing and oxidizing atmospheres while maintaining a high ionic conductivity on the one hand and low electronic conductivity on the other, especially under reducing atmospheres. For high temperature SOFC, yttria stabilized zirconia (YSZ), with the fluorite structure, represents the present state-of-the-art material. Sr- and Mg-doped $LaGaO_3$ (LSGM) perovskites are some of the most promising alternatives to YSZ [30,31]. The high ionic conductivity is obtained in $LaGaO_3$ when doping simultaneously on the A and B perovskite sites with a lower valence cation. The maximum ionic conductivity for these systems is reached for $La_{0.8}Sr_{0.2}Ga_{0.8}Mg_{0.2}O_{3-\delta}$ [32] although several other interesting variations have also been reported [33–37] to show high performance at intermediate temperature.

In the present work, we show the effect of A-site doping La_2NiTiO_6 with Sr. This oxide belongs to the "double perovskite" family, a particular case of a perovskite with general formula $A_2BB'O_6$ which are known to display a huge variety of compositions and properties related to their capability of accommodating different transition-metal cations B and B' of different sizes and electronic structures [14]. The compounds $La_{2-x}Sr_xNiTiO_{6-\delta}$ have been fully characterized by both structural and electrochemical methods to assess their potential as SOFC electrodes in view of the electrochemical performance. Thermal and chemical stability (under oxidizing and reducing conditions) are presented together with a compatibility study with other materials commonly used in SOFC technology.

2. Materials and methods

2.1. Samples

The synthesis of samples $La_{2-x}Sr_xNiTiO_{6-\delta}$ (x = 0 –LSNT00–, 0.10 –LSNT10–, 0.15 –LSNT15–, 0.20 –LSNT20–, 0.25 –LSNT25– and 0.50 –LSNT50–) was carried out by a modified Pechini method. Approximately 10 g of each composition were prepared by dissolving stoichiometric amounts of high-purity Ni (Aldrich 99.99%), La_2O_3 (Alfa Aesar, 99.9%) and $SrCO_3$ (Aldrich 99.9%) in ca. 20 ml of concentrated hot nitric acid (Panreac 66%), before adding 50 ml of distilled water. Citric acid was subsequently added in a 3:1 molar ratio of citric acid: metal ions in conditions of constant heating and vigorous stirring. Non-soluble TiO_2 (anatase, Aldrich 99.9%) was then added to obtain a homogeneous suspension. Once the solution had reduced to half the initial volume, 3 ml of diethylene glycol was added to promote polymerization. The resulting

Please cite this article in press as: Pérez-Flores JC, et al., Structural and electrochemical characterization of $La_{2-x}Sr_xNiTiO_{6-\delta}$, International Journal of Hydrogen Energy (2011), doi:10.1016/j.ijhydene.2011.10.101

solid resin was cooled to room temperature, milled in an agate mortar and the powder burnt at 1073 K to remove the organic matter. After milling and homogenization, the resulting powder was fired at 1773 K for 24 h and cooled at a rate of 2 K min^{-1} to room temperature to obtain well crystallized materials.

Reduced samples were obtained from the samples prepared under air (see above) by heating at 1225 K for 12 h (2 K min^{-1}) under a 5%H_2/N_2 stream in dry conditions ($pO_2 \sim 10^{-21}$ atm) or wet conditions, achieved by bubbling in water at room temperature ($pO_2 \sim 10^{-17}$ atm).

2.2. Experimental techniques

Purity and structure of the samples were determined by powder X-ray diffraction (XRD) on a Bruker D8 high-resolution diffractometer, using monochromatic $CuK_{\alpha 1}$ ($\lambda = 1.5406$ Å) radiation obtained with a germanium primary monochromator, and equipped with a solid-state rapid LynxEye detector. For structure refinement, the measured angular range, step size and counting times were selected to ensure sufficient resolution.

Neutron powder diffraction (NPD) experiments at room temperature were performed on the diffractometer D1A at Institut Laue-Langevin. In order to access long Q values, a monochromatic beam of wavelength 1.3893 Å was selected with a Ge monochromator; for this radiation the instrumental resolution is within the range $2.7 \times 10^{-3} \leq (\Delta Q/Q) \leq 0.022$. The structural refinements were carried out by the Rietveld method using the FullProf program [38] by the simultaneous fitting of XRD and NPD data. The neutron scattering amplitudes used in the refinement were 0.824, 0.702, 1.03, −0.344 and 0.581 × (10^{-12} cm) for La, Sr, Ni, Ti and O, respectively. Prior to structure refinement, a pattern matching without structural model was performed to obtain suitable profile parameters. The structural model was then refined keeping constant the profile parameters. If needed, throughout the refinements some of the profile parameters were allowed to vary; however, during the final steps of the refinements they were kept constant. The refinements were stable provided the number of refined parameters describing the structural model was low enough to obtain an adequate peaks-to-parameters ratio. To ensure this, isotropic thermal factors (ITF) were employed for all the atoms in the structure and some additional constrains were used: the metal sites were considered fully occupied and the same thermal factor was used for all oxygen atoms. The fitting process was finished when convergence was reached.

Thermal expansion coefficients were calculated for as-prepared samples from a series of XRD patterns recorded in air as a function of temperature from RT to 1300 K every 50 K. The unit cell parameters were obtained by Le Bail fitting of these data. The thermal-expansion coefficients along the cell axes *a*, *b* and *c* were determined as $\alpha_{i=a,b,c} = \Delta i/(\Delta T \times i)$, whereas the volumetric thermal-expansion coefficient is given by $\alpha_V = \Delta V/(\Delta T \times V)$, where $(\Delta i/\Delta T)_{i=a,b,c}$ and $(\Delta V/\Delta T)$ are obtained as the slope of linear fit of the corresponding axis or cell volume against *T*, and $i = a, b, c$ or *V* are the RT values.

Slurries for symmetrical cell measurements were prepared by mixing the as-prepared LSNT20, LSNT50 and LSM (Next-Tech) powders with YSZ (Pi-KEM) in a 1:1 ratio with Decoflux™ (WB41, Zschwimmer and Schwartz) as a binder. The electrodes were prepared by coating dense YSZ disks (thickness, 1 mm) with these slurries using active areas of 10 mm^2. The resulting assemblies were fired at 1423 K for 10 h and then a Pt-based paste was deposited on top of the electrodes and fired at 1173 K for 2 h.

Electrode microstructure was investigated using a 6490L JEOL Scanning Electron Microscope.

The polarization measurements were performed on a two-electrode arrangement as previously described [39] using flows of either pure oxygen or a 5%H_2/N_2 mixture to create different atmospheres in the 973–1223 K temperature range. AC impedance spectroscopy measurements of the electrochemical cell were carried out using a 1470E Solartron Cell Test in the frequency range 10^{-1}–10^6 Hz using an AC signal amplitude of 50 mV.

3. Results and discussion

3.1. Thermal expansion

Fig. 1 shows the XRD patterns obtained for the dimensional stability study of LSNT25. No significant decomposition or

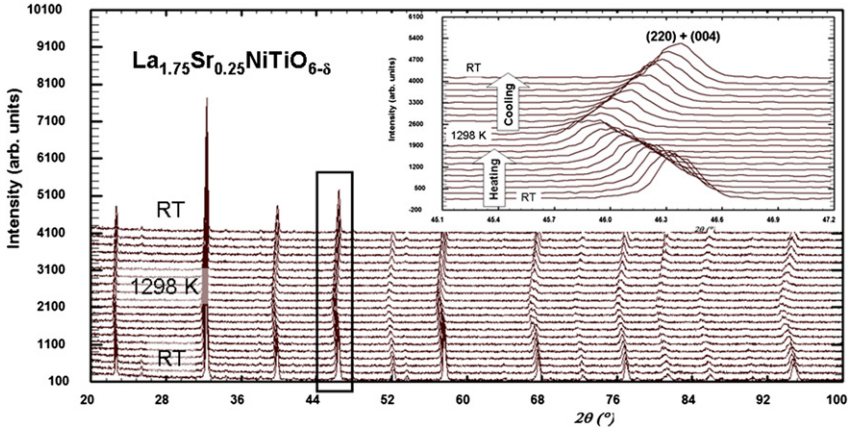

Fig. 1 – XRD patterns of $La_{1.75}Sr_{0.25}NiTiO_{6-\delta}$ recorded at different temperatures. The inset shows the 2θ range corresponding to the (220) and (004) Bragg peaks.

Please cite this article in press as: Pérez-Flores JC, et al., Structural and electrochemical characterization of $La_{2-x}Sr_xNiTiO_{6-\delta}$, International Journal of Hydrogen Energy (2011), doi:10.1016/j.ijhydene.2011.10.101

structural change is appreciated for this sample in the temperature range investigated (973–1223 K). Accordingly to the Sr-content [40], the material presents orthorhombic symmetry (S.G. Pnma) at RT which is maintained in the mentioned temperature range, as can be inferred from Fig. 1. Thus, the sole effect of heating is cell expansion. This is made evident by the displacement of the Bragg peaks to lower angles; in the inset of Fig. 1 this is depicted for the (220) and (004) reflections. Notably, no splitting of the (220) peaks is observed, which rules out that any monoclinic distortion occurs upon heating.

For LSNT25, the linear expansion coefficients along the cell axis, α_a, α_b and α_c are 10.2(1) $\times$ 10^{-6}, 12.4(2) $\times$ 10^{-6} and 6.7(1) $\times$ 10^{-6} K^{-1} respectively, whereas the volumetric coefficient is $\alpha_V = 30.0(5) \times 10^{-6}$ K^{-1}. According to these values, the material can be considered to be essentially isotropic, and therefore the linear thermal expansion coefficient, α_L, can be approximated by the general expression $\alpha_V = 3\alpha_L$ and $\alpha_L = 10.0(3) \times 10^{-6}$ K^{-1}. Very similar values are found for all samples studied, regardless of the strontium content. Interestingly, typical SOFC materials such as YSZ (electrolyte), cermet 30%Ni/YSZ (anode), LSM (cathode), LSC (ceramic

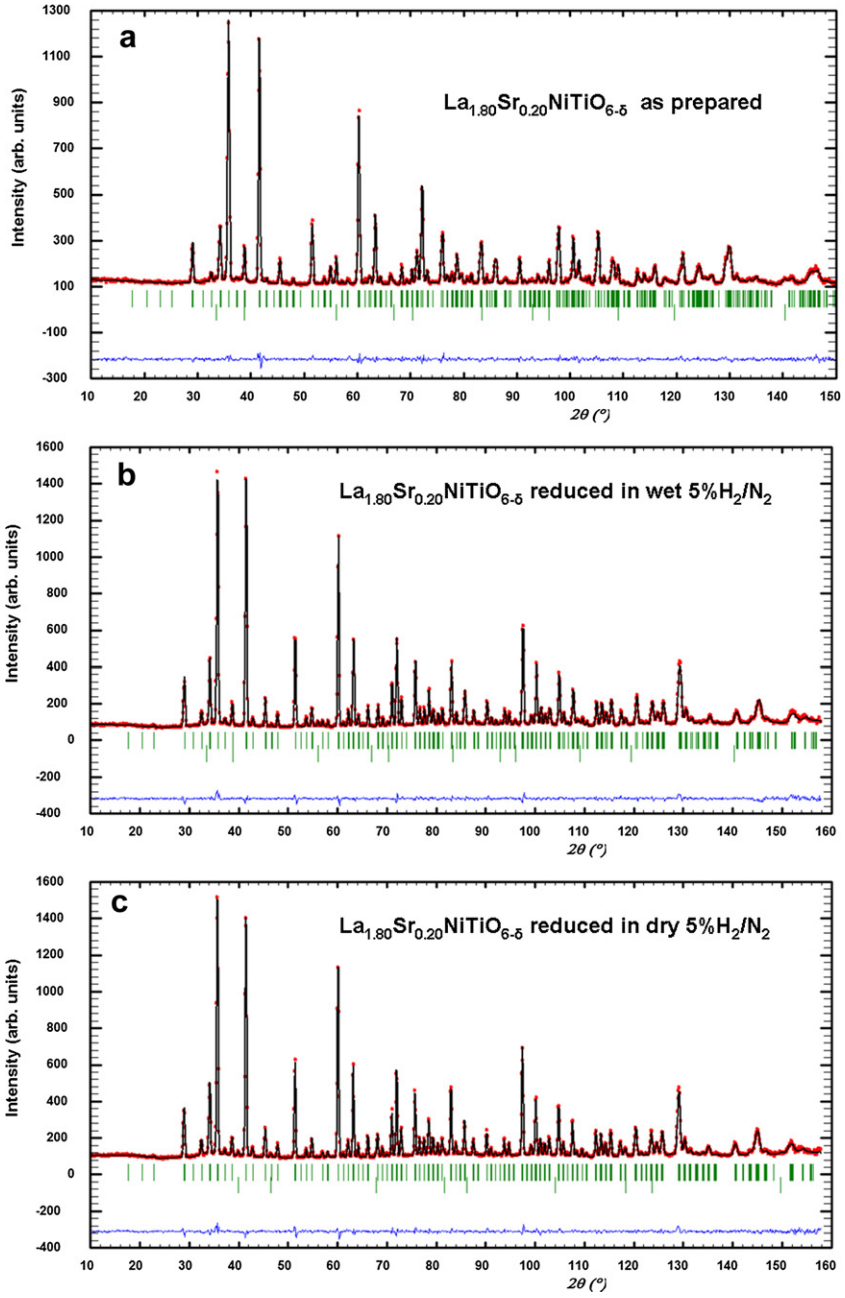

Fig. 2 – Experimental (points), calculated (continuous line) NPD patterns and their difference (bottom) for: (a) as-prepared $La_{1.80}Sr_{0.20}NiTiO_{6-\delta}$ (b) after reduction in wet 5%H_2/N_2, and (c) reduced in dry 5%H_2/N_2. In all cases, the first row of vertical bars indicates the Bragg peaks of the major perovskite phase in (a) and (b) the second row indicates the positions of the maxima corresponding to c.a. 3% NiO, and in (c) the second row indicates Ni metal (maxima ca. 3%).

Please cite this article in press as: Pérez-Flores JC, et al., Structural and electrochemical characterization of $La_{2-x}Sr_xNiTiO_{6-\delta}$, International Journal of Hydrogen Energy (2011), doi:10.1016/j.ijhydene.2011.10.101

interconnector) and Fe/18–24%Cr (metallic interconnector) exhibit similar values of α_L, typically in the range 10.5–14 × 10^{-6} K^{-1} [41–43]. Therefore, the title oxides are thermally and mechanically compatible with most used SOFC materials, and also have comparable expansion coefficients to those of the main perovskite-type alternatives for SOFCs [15,44,45].

3.2. *Chemical stability and compatibility*

3.2.1. *Chemical stability*

Any material to be used as an SOFC component must be stable under working conditions. Thus, anode compounds require stability in reducing atmospheres; materials to be used as cathodes must be stable in oxidizing conditions, whereas electrolytes are required to suffer no evolution/reaction in either type of atmosphere.

Since the title compounds are prepared at high temperature in air (pO_2 = 0.21 atm) their stability in oxidizing environments is evident, as confirmed by XRD (Fig. 1). However, their behavior under reducing conditions is hitherto unknown and has been investigated. Representative samples of $La_{2-x}Sr_xNiTiO_{6-\delta}$ with $x = 0.2$ and 0.5 were heated and reduced in dry and wet 5%H_2/N_2 streams overnight (see experimental section for details) and then characterized by NPD at RT. The refined structural parameters of the as-prepared and the reduced materials were obtained by simultaneous fitting of XRD and NPD data. Fig. 2 shows the corresponding NPD patterns for $La_{1.80}Sr_{0.20}NiTiO_{6-\delta}$; structural parameters are listed in Table 1, and Table 2 presents some additional structural information.

As previously reported [40], oxides of the $La_{2-x}Sr_xNiTiO_{6-\delta}$ series present perovskite-like structures with unit cell $\sqrt{2}a_p \times \sqrt{2}a_p \times 2a_p$ (where a_p refers to the cell of the simple cubic perovskite), either monoclinic (S.G. $P2_1/n$, #14) for low Sr-content ($x \leq 0.10$) or orthorhombic (S.G. Pnma, #62) for $x > 0.1$. The reason for this lowering in symmetry is mainly due to the ordering of Ti and Ni on the B positions of the structure. Both compositions studied in this work show orthorhombic symmetry and hence cation disordering within the perovskite B-sites. A random distribution of Sr and La (and possibly of the oxygen vacancies which are created by aliovalent

Table 1 – Structural parameters for reduced $La_{2-x}Sr_xNiTiO_{6-\delta}$ (x = 0.20, 0.50) obtained from NPD data.

	$La_{1.80}Sr_{0.20}NiTiO_{6-\delta}$			$La_{1.50}Sr_{0.50}NiTiO_{6-\delta}$		
	As prepared[a]	Wet 5%H_2/N_2[b]	Dry 5%H_2/N_2[c]	As prepared[d]	Wet 5%H_2/N_2[e]	Dry 5%H_2/N_2[f]
a (Å)	5.5395(2)	5.5380(1)	5.5438(1)	5.5200(2)	5.5250(1)	5.5268(1)
b (Å)	7.8294(2)	7.8289(1)	7.8370(1)	7.8104(4)	7.8188(1)	7.8229(1)
c (Å)	5.5480(2)	5.5480(1)	5.5516(1)	5.5451(2)	5.5508(1)	5.5524(1)
V (Å^3)	240.62(5)	240.54(6)	241.20(4)	239.07(4)	239.79(3)	240.06(4)
0.5						
La/Sr position 4c						
Occ La/Sr[g]	0.450(1)/0.050(1)	0.450(1)/0.050(1)	0.450(1)/0.050(1)	0.373(2)/0.127(2)	0.375(3)/0.125(2)	0.375(3)/0.125(2)
x	0.0248(3)	0.0239(2)	0.0248(3)	0.0156(6)	0.0125(4)	0.0103(5)
z	0.0057(6)	0.0039(5)	0.0044(5)	0.0032(3)	0.0016(6)	0.0014(7)
$U \times 100$ (Å^2)	0.94(3)	0.84(2)	0.89(2)	1.15(4)	0.93(3)	1.10(5)
0.5						
B position 4b						
Occ Ni/Ti[g]	0.241(1)/0.259(1)	0.249(1)/0.251(1)	0.248(1)/0.252(1)	0.230(4)/0.270(4)	0.228(4)/0.272(4)	0.227(4)/0.273(4)
$U \times 100$ (Å^2)	0.08(2)	0.79(4)	0.60(4)	0.11(3)	0.59(3)	0.82(3)
0.5						
O(1) position 4c						
x	0.4902(6)	0.4888(4)	0.4889(5)	0.493(1)	0.4919(8)	0.495(1)
z	−0.0680(6)	−0.0684(5)	−0.0693(5)	−0.0606(8)	−0.0621(5)	−0.0606(4)
Occ[g]	0.50(1)	0.50(1)	0.49(1)	0.49(1)	0.49(1)	0.49(1)
$U \times 100$ (Å^2)	0.80(2)	0.64(2)	0.82(3)	0.92(3)	1.01(4)	1.08(6)
0.5						
O(2) position 8d						
x	0.2814(4)	0.2806(3)	0.2810(3)	0.2755(6)	0.2722 (4)	0.2716(4)
y	0.4644(3)	0.4640(2)	0.4632(2)	0.4667(4)	0.4667(2)	0.4661(2)
z	0.2794(4)	0.2789(3)	0.2796(3)	0.2726(6)	0.2697(4)	0.2710(5)
Occ[g]	0.98(1)	0.99(1)	0.97(2)	0.95(1)	0.94(1)	0.93(1)
$U \times 100$ (Å^2)	0.80(2)	0.64(2)	0.82(3)	0.92(3)	1.01(4)	1.08(6)

S.G. Pnma: 4c (x 1/4 z), 4b (0 0 1/2), 8d (x y z).
a $\chi^2 = 1.97$, $R_{wp} = 9.20\%$, $R_{exp} = 6.55\%$, $R_B = 2.63\%$, Composition: 97(1)% w $La_{1.800(2)}Sr_{0.200(2)}Ni_{0.964(2)}Ti_{1.036(2)}O_{5.92(4)}$, 3(1)% w NiO.
b $\chi^2 = 1.67$, $R_{wp} = 8.43\%$, $R_{exp} = 6.52\%$, $R_B = 3.66\%$, Composition: 97(1)% w $La_{1.800(2)}Sr_{0.200(2)}Ni_{0.996(5)}Ti_{1.004(5)}O_{5.96(4)}$, 3(1)% w NiO.
c $\chi^2 = 1.48$, $R_{wp} = 8.51\%$, $R_{exp} = 7.00\%$, $R_B = 3.12\%$, Composition: 98(1)% w $La_{1.800(2)}Sr_{0.200(2)}Ni_{0.992(5)}Ti_{1.008(5)}O_{5.84(8)}$, 2(1)% w Ni.
d $\chi^2 = 3.18$, $R_{wp} = 7.03\%$, $R_{exp} = 3.92\%$, $R_B = 5.00\%$, Composition: 97(1)% w $La_{1.492(2)}Sr_{0.508(2)}Ni_{0.920(5)}Ti_{1.080(5)}O_{5.76(3)}$, 3(1)% w NiO.
e $\chi^2 = 1.20$, $R_{wp} = 9.77\%$, $R_{exp} = 8.90\%$, $R_B = 4.26\%$, Composition: 97(1)% w $La_{1.500(3)}Sr_{0.500(3)}Ni_{0.912(5)}Ti_{1.088(5)}O_{5.72(3)}$, 3(1)% w NiO.
f $\chi^2 = 1.24$, $R_{wp} = 11.0\%$, $R_{exp} = 8.91\%$, $R_B = 5.24\%$, Composition: 97(1)% w $La_{1.500(3)}Sr_{0.500(3)}Ni_{0.901(5)}Ti_{1.092(5)}O_{5.68(5)}$, 3(1)% w Ni.
g The occupancy values are given as the multiplicity of the position divided by the general multiplicity of the space group.

Please cite this article in press as: Pérez-Flores JC, et al., Structural and electrochemical characterization of $La_{2-x}Sr_xNiTiO_{6-\delta}$, International Journal of Hydrogen Energy (2011), doi:10.1016/j.ijhydene.2011.10.101

Table 2 – Selected structural information for the title samples obtained from NPD data. Angles are given in degrees and distances in Å, distortion Δ of the BO_n polyhedra and bond valence sums [51] are reported. $\Delta = 1/n\Sigma_{j=1,n}\{(d_n - <d>)/<d>\}^2$ where $<d>$ is the average B–O distance.

	$La_{1.80}Sr_{0.20}NiTiO_{6-\delta}$			$La_{1.50}Sr_{0.50}NiTiO_{6-\delta}$		
	As prepared	Wet 5%H_2/N_2	Dry 5%H_2/N_2	As prepared	Wet 5%H_2/N_2	Dry 5%H_2/N_2
Tilt angle θ[a]	10.6(3)	10.6(3)	10.8(3)	9.3(3)	8.9(3)	9.1(3)
Tilt angle ϕ[b]	10.6(3)	10.6(3)	10.8(3)	9.3(3)	8.9(3)	9.1(3)
Tilt angle μ[c]	11.1(3)	11.1(3)	11.2(3)	9.8(3)	10.1(3)	9.8(3)
B-O(1) × 2	1.995(1)	1.995(1)	1.997(1)	1.982(1)	1.985(1)	1.985(1)
B-O(2) × 2	1.987(3)	1.987(3)	1.992(2)	1.972(3)	1.973(2)	1.982(2)
B-O(2) × 2	2.000(3)	2.000(2)	2.001(2)	1.993(3)	1.991(2)	1.985(2)
Average B–O	1.994(2)	1.994(1)	1.997(1)	1.982(1)	1.983(1)	1.984(1)
Distortion $B–O_6 \times 10^4$	0.073	0.061	0.038	0.182	0.140	0.005
B BVS (Ni/Ti)	2.65(2)/4.01(2)	2.65(1)/4.01(1)	2.58(1)/3.99(1)	2.70(2)/4.13(2)	2.70 (2)/4.12(2)	2.67(3)/4.10 (3)

a With [110] for $P2_1/n$; with [101] for Pnma.
b With [1–10] for $P2_1/n$; with [10–1] for Pnma.
c With [001] for $P2_1/n$; with [010] for Pnma.

substitution) is expected to provide the driving force for disordering of Ni and Ti.

Interestingly, our samples seem to be slightly Ni-deficient and a small amount of NiO (~1 wt.%) was detected by NPD (but not by XRD) associated with a slight Ti over-stoichiometry (Table 1).

All of the $La_{2-x}Sr_xNiTiO_{6-\delta}$ phases exhibit perovskite tolerance factors below unity leading to a tilting of the BO_6 octahedra. In the Glazer notation [46,47], the tilting system is $a^-a^-c^+$, irrespective of monoclinic or orthorhombic symmetry, indicating that octahedra rotate along the Cartesian axes *x* and *y* in consecutive layers in opposite directions, and along the *z*-axis in the same direction. The octahedral tilts can be calculated from the B–O–B bond angles (ω) as $(180 - \omega)/2$; the tilt values obtained from the NPD data are given in Table 2. The tolerance factor increases slightly with increasing Sr content; as a result, the tilting angles of the octahedra decrease and the structure becomes more regular and symmetric.

Both metal–oxygen distances and bond-valence sums (BVS) in Table 2 support the cation distribution determined by NPD (Table 1). For a high-enough degree of substitution of La^{3+} by Sr^{2+}, Ti^{4+} and Ni^{2+} are disordered, as reflected by the convergence of both B–O distances and the BVS of the B positions.

Aliovalent substitution of La^{3+} by Sr^{2+} may induce different charge-compensation mechanisms; these include oxidation of Ni^{2+} to Ni^{3+}

$$xSrO(La_2NiTiO_6) \rightarrow xSr'_{La} + xNi^{\cdot}_{Ni} \quad (1)$$

and creation of oxygen vacancies

$$xSrO(La_2NiTiO_6) \rightarrow xSr'_{La} + x/2V^{\cdot\cdot}_{O} \quad (2)$$

The first process can be discarded [40] as the main charge-compensating mechanism, as the amount of Ni^{3+} in $La_{2-x}Sr_xNiTiO_{6-\delta}$ is quite low. The existence of oxygen vacancies in $La_{2-x}Sr_xNiTiO_{6-\delta}$ is confirmed by NPD; as Table 1 shows, the refined oxygen content decreases with increasing Sr-doping.

Concerning the reduced samples, it is worth noting that both $La_{1.80}Sr_{0.20}NiTiO_{6-\delta}$ (Fig. 2) and $La_{1.50}Sr_{0.50}NiTiO_{6-\delta}$ are stable upon reduction, independently of the mild or extreme reducing conditions used (wet or dry 5%H_2/N_2 – $pO_2 \approx 10^{-17}$ or 10^{-21} atm). The only observable effect induced in the materials by these reducing conditions is a slight increase of the unit cell volume (0–0.2%) associated with a small release of oxygen (Table 1) and with the reduction of Ni^{3+} to Ni^{2+} (see

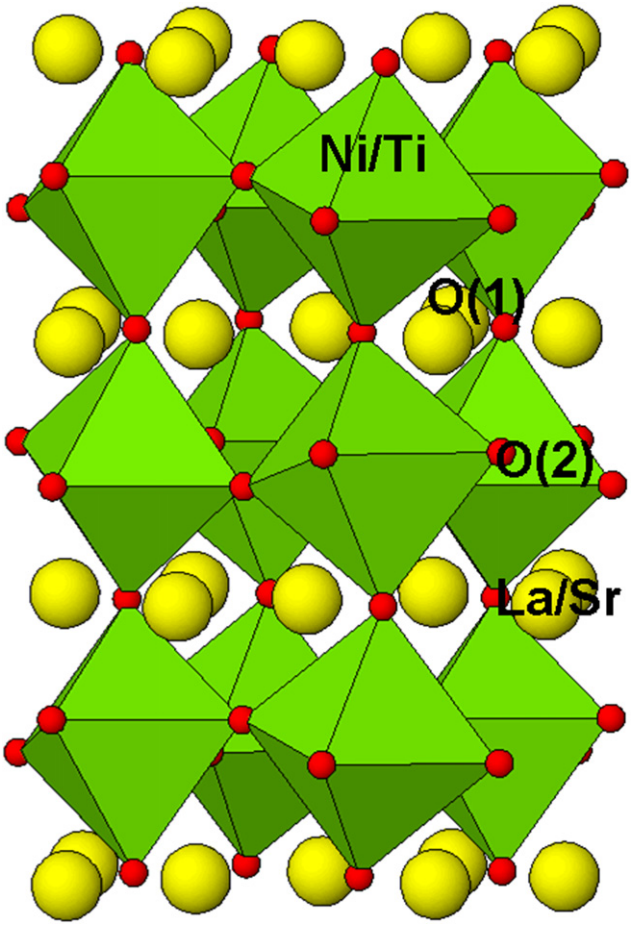

Fig. 3 – Schematic representation of the structure of $La_{2-x}Sr_xNiO_{6-\delta}$ for $x \geq 0.20$ in Pnma symmetry.

Please cite this article in press as: Pérez-Flores JC, et al., Structural and electrochemical characterization of $La_{2-x}Sr_xNiTiO_{6-\delta}$, International Journal of Hydrogen Energy (2011), doi:10.1016/j.ijhydene.2011.10.101

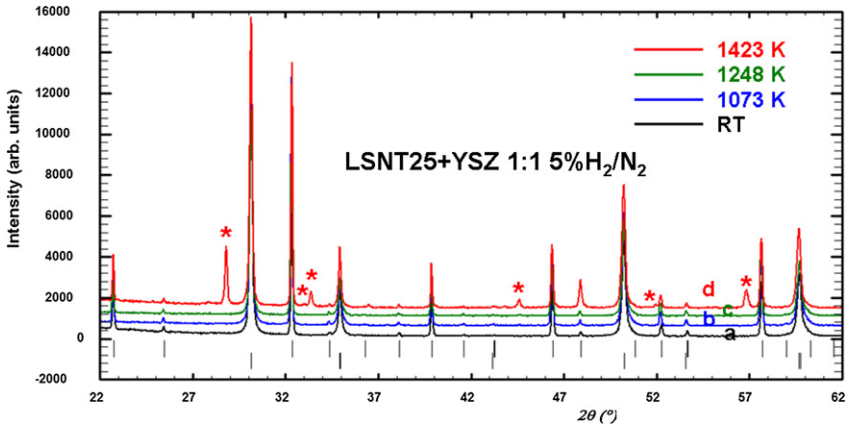

Fig. 4 – XRD patterns of a mixture of LSNT25/YSZ in 1:1 ratio (a) before and after treatment overnight at (b) 1073 K, (c) 1248 K and (d) 1342 K in 5%H_2/N_2. In the latter case, peaks corresponding to an unidentified impurity phase are indicated by asterisks. The first and second rows of vertical bars indicate the positions of Bragg peaks of LSNT25 and YSZ, respectively.

BVS in Table 2). As shown in Table 1, oxygen seems to be preferentially removed from O(2) positions (site 8c), which correspond to those located in the Ni/Ti layers (Fig. 3) whereas O(1) positions remain fully occupied.

These effects are more pronounced in the sample with higher Sr-content and for more severe reducing treatments. Indeed, samples treated under a 5%H_2/N_2 dry stream experience a volume expansion ca. 0.2–0.4% and an oxygen release around 1.4%. The refined structural parameters in Tables 1 and 2 confirm the preferential loss of oxygen in the 8c site, associated with the reduction of trivalent nickel, which induces an elongation of the B–O distances. On the other hand, no significant variation of the octahedral tilting is observed.

Finally, in Fig. 2 the most striking effect of reducing treatments on samples is the reduction of the small quantity of the impurity, NiO (see above) under very high reducing conditions (dry 5%H_2/N_2) to yield some metallic nickel. However, the amounts of NiO or Ni are as small as 2–3% in weight, and will have no (or little) influence on the observed properties of the samples.

3.2.2. *Chemical compatibility under working conditions*

The chemical compatibility of $La_{2-x}Sr_xNiTiO_{6-\delta}$ oxides used as electrode components with YSZ was evaluated by mixing either LSNT25 or LSNT50 with YSZ in a 1:1 w:w ratio. The mixtures were pelletized and heated at 1073, 1248 and 1423 and K for 15 h under either oxidizing atmospheres or reducing conditions of 5%H_2/N_2. These temperatures were chosen as representative of the SOFC working and processing conditions: the former as operating temperature, the latter as electrode fabrication temperature and an intermediate one (1248 K). After the treatments the samples were checked by XRD.

As an example, Fig. 4 shows the XRD patterns corresponding to LSNT25:YSZ (1:1) mixture treated under reducing atmosphere. It is clear that no decomposition or reaction occurs under such working conditions; however, at high temperatures (1428 K, far from those needed for operating the cell) some decomposition or reaction is observed, since unidentified peaks are observed. Notably, the electrodes are prepared in air and usually such strong reducing conditions are not applied under operation.

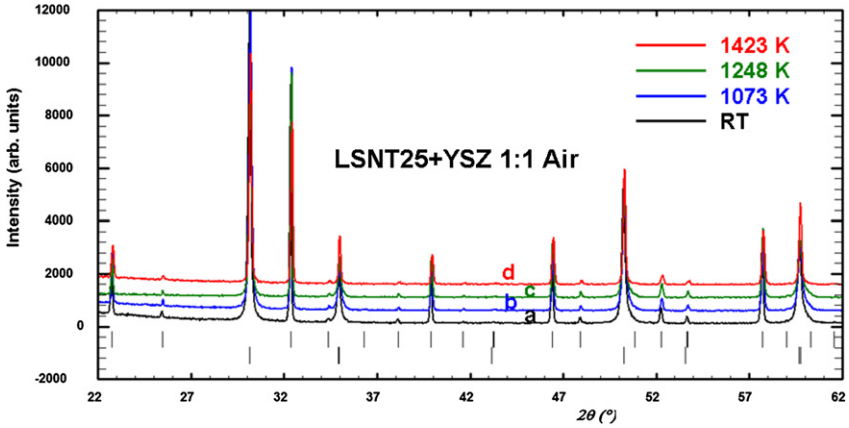

Fig. 5 – XRD patterns of a mixture of LSNT25/YSZ in 1:1 ratio before (a) and after treatment overnight at (b) 1073 K, (c) 1248 K and (d) 1342 K in air. The first and second rows of vertical bars indicate the positions of Bragg peaks of LSNT25 and YSZ, respectively.

Please cite this article in press as: Pérez-Flores JC, et al., Structural and electrochemical characterization of $La_{2-x}Sr_xNiTiO_{6-\delta}$, International Journal of Hydrogen Energy (2011), doi:10.1016/j.ijhydene.2011.10.101

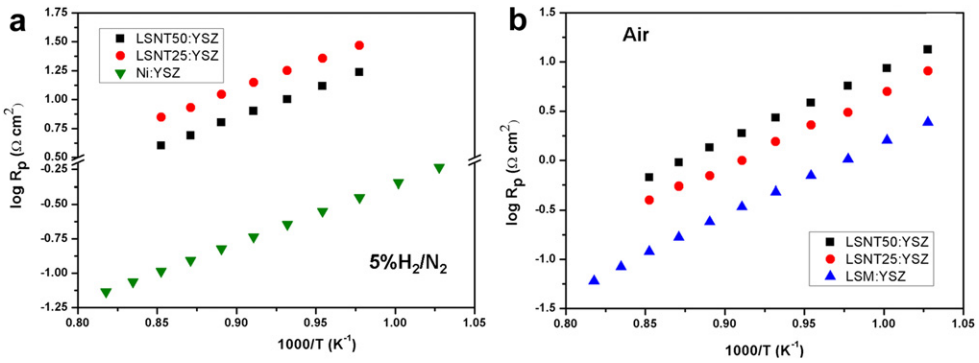

Fig. 6 – Temperature dependence of the polarization resistance of LSNT25 and LSNT50 symmetric cells under (a) anode and (b) cathode conditions. The data for Ni-YSZ cermet were obtained from Atkinson et al. [48].

Therefore, the reaction/decomposition observed would not inhibit the possible use of the studied material as an anode in SOFCs.

Fig. 5 shows the results of chemical compatibility of LSNT25 with YSZ in an oxidizing atmosphere (air), i.e. under the conditions in the cathode side. In this case, no reaction or decomposition is observed at these temperatures. The possible use of the title materials in the cathode side would present even less chemical or compatibility problems than in the anode.

3.3. *Electrochemical performance*

The electrochemical tests performed on symmetrical cells revealed that LSNT-based electrodes exhibited relatively high polarization resistances under both reducing and oxidizing atmospheres (Fig. 6), e.g. 1.5 Ω cm^2 in oxygen and higher than 15 Ω cm^2 in 5%H_2/N_2 at 1073 K.

According to the reference values for the most commonly used anode, Ni-YSZ cermet [48], under reducing conditions, the electrochemical performances are particularly poor (Fig. 6a), which indicates that these families of compounds cannot be used as SOFC anodes.

Interestingly, under oxidizing conditions (Fig. 6b), though the polarization resistances are higher than in LSM-based cathodes, which show polarizations below 0.5 Ω cm^2 at the same temperature, the values are close to those previously reported for other materials [49]. Nevertheless, the R_p values of the materials reported suggest a poor electrochemical response for oxygen reduction and therefore low interest of the materials as SOFC cathodes. We note, however, that although the overall conductivity of LSNT materials is modest and hence may be partly responsible for the high polarization values, there are some extrinsic factors which clearly contribute to an increased polarization resistance. It is well known that the microstructure plays a crucial role in the electrochemical performance of fuel cell electrodes as it should allow an efficient transfer of gases to/from the active sites. In the present case, SEM micrographs (Fig. 7) before testing reveal adequate thickness (ca. ~50 μm) and porosity distribution. In general, the micrographs show a good contact between the electrode and the electrolyte with high homogeneity in particle size distribution; however some regions observed in a cross-section view show the presence of large cavities, which may have a detrimental effect on mass transport and therefore result in somewhat larger polarization values (inset of Fig. 7). In these regions, the decrease of contact area and adhesion losses will reduce the electron motion and oxide ion diffusion, and as a result the polarization resistance will increase. It should be noted too, that although the XRD-chemical compatibility studies do not show any undesirable reaction with the electrolyte, as previously commented, the possibility of cationic species diffusing across the interface between the electrode and electrolyte components cannot be ruled out, which could also lead to increasing polarization effects.

Another possibility to improve the cathode polarization is related with intrinsic factors. It is well known that the B-site element plays an important role on the catalytic activity of perovskites. In particular cobalt is more efficient than Ni for oxygen reduction reactions [44,50]. Therefore, further work is needed to optimize the chemical composition and electrode fabrication process to improve the performance of LSNT-based electrodes.

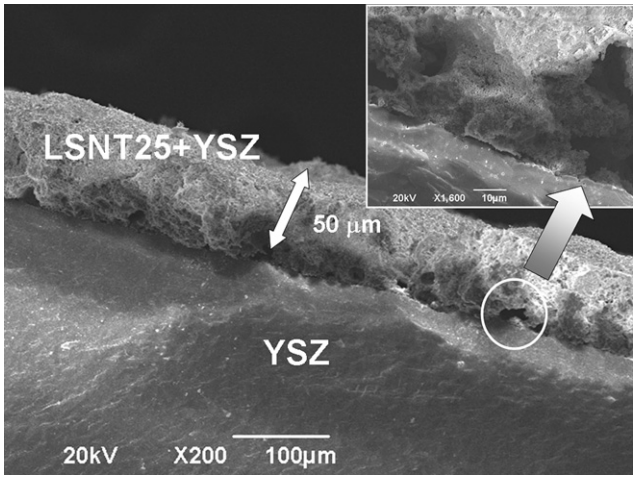

Fig. 7 – SEM micrograph of the cathode LSNT25/YSZ prepared at 1423 K overnight. The inset shows a detail of a typical void formed which is expected to limit the electrode performance.

Please cite this article in press as: Pérez-Flores JC, et al., Structural and electrochemical characterization of $La_{2-x}Sr_xNiTiO_{6-\delta}$, International Journal of Hydrogen Energy (2011), doi:10.1016/j.ijhydene.2011.10.101

4. Conclusions

The structural characterization of selected compositions of the perovskite series $La_{2-x}Sr_xNiTiO_{6-\delta}$ ($0 \leq x \leq 0.5$) by neutron and X-ray diffraction indicate that they are stable under both oxidizing and reducing conditions. Moreover, an analysis of mixtures with YSZ at different temperatures showed that the investigated perovskites are chemically compatible with the most used electrolytes for SOFC at the maximum operating temperatures (ca. 800 °C and over) in both oxidizing and reducing atmospheres. Thermal expansion of the series was determined to be isotropic with $\alpha_L = 10.0(3) \times 10^{-6}$ K^{-1}. This value is similar to that found for other perovskite materials used in SOFC. The preliminary evaluation of the electrode performance reveals modest polarization resistances of 1.5 Ω cm^2 in oxygen at 1073 K. On the other hand, the results under reducing atmosphere indicate a rather poor electrochemical response, i.e. 15 Ω cm^2 at the same temperature. Nevertheless, microstructure and chemical composition have not been optimized fully enough to discard the material as a possible cathode for SOFC.

Acknowledgements

We thank Ministerio de Ciencia e Innovación and Comunidad de Madrid for funding the projects MAT2010-19837-C06-01/-04, PIB2010JP-00181 and S2009/PPQ-1626 respectively. D. Pérez-Coll acknowledges the MCINN and CSIC for a Ramón y Cajal contract.

REFERENCES

[1] Jacobson AJ. Materials for solid oxide fuel cells. Chemistry of Materials 2009;22(3):660–74.
[2] Adler SB. Factors governing oxygen reduction in solid oxide fuel cell cathodes. Chemical Reviews 2004;104(10):4791–844.
[3] Ormerod RM. Solid oxide fuel cells. Chemical Society Reviews 2003;32(1):17–28.
[4] Tsipis E, Kharton V. Electrode materials and reaction mechanisms in solid oxide fuel cells: a brief review. Journal of Solid State Electrochemistry 2008;12(9):1039–60.
[5] Goodenough JB, Huang Y-H. Alternative anode materials for solid oxide fuel cells. Journal of Power Sources 2007;173(1):1–10.
[6] Sun C, Stimming U. Recent anode advances in solid oxide fuel cells. Journal of Power Sources 2007;171(2):247–60.
[7] Mogensen M, Lybye D, Bonanos N, Hendriksen PV, Poulsen FW. Factors controlling the oxide ion conductivity of fluorite and perovskite structured oxides. Solid State Ionics 2004;174(1–4):279–86.
[8] Fergus JW. Oxide anode materials for solid oxide fuel cells. Solid State Ionics 2006;177(17, 18):1529–41.
[9] Orera A, Slater PR. New chemical systems for solid oxide fuel cells. Chemistry of Materials 2009;22(3):675–90.
[10] Liu Z, Han M-F, Miao W- T. Preparation and characterization of graded cathode $La_{0.6}Sr_{0.4}Co_{0.2}Fe_{0.8}O_{3-\delta}$. Journal of Power Sources 2007;173(2):837–41.
[11] Sun X, Wang S, Wang Z, Qian J, Wen T, Huang F. Evaluation of $Sr_{0.88}Y_{0.08}TiO_3$–CeO_2 as composite anode for solid oxide fuel cells running on CH_4 fuel. Journal of Power Sources 2009;187(1):85–9.
[12] Orlovskaya N, Lugovy M, Pathak S, Steinmetz D, Lloyd J, Fegely L, et al. Thermal and mechanical properties of LaCoO3 and La0.8Ca0.2CoO3 perovskites. Journal of Power Sources 2008;182(1):230–9.
[13] Yamaji K, Horita T, Ishikawa M, Sakai N, Yokokawa H. Chemical stability of the $La_{0.9}Sr_{0.1}Ga_{0.8}Mg_{0.2}O_{2.85}$ electrolyte in a reducing atmosphere. Solid State Ionics 1999;121(1–4):217–24.
[14] Jiang S. Development of lanthanum strontium manganite perovskite cathode materials of solid oxide fuel cells: a review. Journal of Materials Science 2008;43(21):6799–833.
[15] Sun C, Hui R, Roller J. Cathode materials for solid oxide fuel cells: a review. Journal of Solid State Electrochemistry 2010;14(7):1125–44.
[16] Jiang SP. A comparison of O2 reduction reactions on porous (La, Sr)MnO_3 and (La, Sr)(Co, Fe)O_3 electrodes. Solid State Ionics 2002;146(1, 2):1–22.
[17] Mai A, Haanappel VAC, Uhlenbruck S, Tietz F, Stöver D. Ferrite-based perovskites as cathode materials for anode-supported solid oxide fuel cells: Part I. Variation of composition. Solid State Ionics 2005;176(15, 16):1341–50.
[18] Tsai T, Barnett SA. Increased solid-oxide fuel cell power density using interfacial ceria layers. Solid State Ionics 1997;98(3, 4):191–6.
[19] Adler SB. Limitations of charge-transfer models for mixed-conducting oxygen electrodes. Solid State Ionics 2000;135(1–4):603–12.
[20] Brichzin V, Fleig J, Habermeier HU, Cristiani G, Maier J. The geometry dependence of the polarization resistance of Sr-doped LaMnO3 microelectrodes on yttria-stabilized zirconia. Solid State Ionics 2002;152, 153:499–507.
[21] Peña MA, Fierro JLG. Chemical structures and performance of perovskite oxides. Chemical Reviews 2001;101(7):1981–2018.
[22] Richter J, Holtappels P, Graule T, Nakamura T, Gauckler L. Materials design for perovskite SOFC cathodes. Monatshefte für Chemie/Chemical Monthly 2009;140(9):985–99.
[23] Yin Y-M, Xiong M-W, Yang N-T, Tong Z, Guo Y-Q, Ma Z-F, et al. Investigation on thermal, electrical, and electrochemical properties of scandium-doped $Pr_{0.6}Sr_{0.4}(Co_{0.2}Fe_{0.8})(1-x)Sc_xO_{3-\delta}$ as cathode for IT-SOFC. International Journal of Hydrogen Energy 2011;36(6):3989–96.
[24] Ghouse M, Al-Yousef Y, Al-Musa A, Al-Otaibi MF. Preparation of $La_{0.6}Sr_{0.4}Co_{0.2}Fe_{0.8}O_3$ nanoceramic cathode powders for solid oxide fuel cell (SOFC) application. International Journal of Hydrogen Energy 2010;35(17):9411–9.
[25] DiGiuseppe G, Sun L. Electrochemical performance of a solid oxide fuel cell with an LSCF cathode under different oxygen concentrations. Int J Hydrogen Energy 2011;36(8):5076–87.
[26] Goodenough JB. Annu Rev Mater Res 2003;33:91–128.
[27] Tao S, Irvine JTS. A redox-stable efficient anode for solid-oxide fuel cells. Nat Mater 2003;2(5):320–3.
[28] Plint SM, Connor PA, Tao S, Irvine JTS. Electronic transport in the novel SOFC anode material $La_{1-x}Sr_xCr_{0.5}Mn_{0.5}O_{3\pm\delta}$. Solid State Ionics 2006;177(19–25):2005–8.
[29] Li X, Zhao H, Xu N, Zhou X, Zhang C, Chen N. Electrical conduction behavior of La, Co co-doped $SrTiO_3$ perovskite as anode material for solid oxide fuel cells. International Journal of Hydrogen Energy 2009;34(15):6407–14.
[30] Ishihara T, Matsuda H, Takita Y. Doped $LaGaO_3$ perovskite type oxide as a new oxide ionic conductor. Journal of the American Chemical Society 1994;116(9):3801–3.
[31] Gomes E, Mather GC, Figueiredo F, Marques FMB. Microstructure and electrical properties of aluminium-substituted La(Sr)Ga(Mg)$O_{3-\delta}$-based solid electrolytes. Monatshefte für Chemie/Chemical Monthly 2009;140(9):1041–52.

Please cite this article in press as: Pérez-Flores JC, et al., Structural and electrochemical characterization of $La_{2-x}Sr_xNiTiO_{6-\delta}$, International Journal of Hydrogen Energy (2011), doi:10.1016/j.ijhydene.2011.10.101

[32] Ishihara T, Matsuda H, Takita Y. Effects of rare earth cations doped for La site on the oxide ionic conductivity of $LaGaO_3$-based perovskite type oxide. Solid State Ionics 1995;79:147–51.
[33] Kharton VV, Yaremchenko AA, Kovalevsky AV, Viskup AP, Naumovich EN, Kerko PF. Perovskite-type oxides for high-temperature oxygen separation membranes. Journal of Membrane Science 1999;163(2):307–17.
[34] Thangadurai VK, Shukla A, Gopalakrishnan J. $La_{0.9}Sr_{0.1}Ga_{0.8}Mn_{0.2}O_{2.85}$: a new oxide ion conductor. Chemical Communications 1998;23:2647–8.
[35] Ishihara T, Shibayama T, Honda M, Nishiguchi H, Takita Y. Intermediate temperature solid oxide fuel cells using $LaGaO_3$ electrolyte II. Improvement of oxide ion conductivity and power density by doping Fe for Ga site of $LaGaO_3$. Journal of the Electrochemical Society 2000;147(4):1332–7.
[36] Ishihara T, Shibayama T, Nishiguchi H, Takita Y. Oxide ion conductivity in $La_{0.8}Sr_{0.2}Ga_{0.8}Mg_{0.2-}XO_3$ perovskite oxide and application for the electrolyte of solid oxide fuel cells. Journal of Materials Science 2001;36(5):1125–31.
[37] Xue J, Shen Y, Zhou Q, He T, Han Y. Combustion synthesis and properties of highly phase-pure perovskite electrolyte Co-doped $La_{0.9}Sr_{0.1}Ga_{0.8}Mg_{0.2}O_{2.85}$ for IT-SOFCs. International Journal of Hydrogen Energy 2010;35(1):294–300.
[38] Rodríguez-Carvajal J. Recent advances in magnetic structure determination by neutron powder diffraction. Physica B: Condensed Matter 1993;192(1, 2):55–69. The program and manual can be found at: http://www.ill.eu/sites/fullprof/.
[39] Ruiz-Morales JC, Canales-Vázquez J, Peña-Martínez J, López DM, Núñez P. On the simultaneous use of $La_{0.75}Sr_{0.25}Cr_{0.5}Mn_{0.5}O_{3-\delta}$ as both anode and cathode material with improved microstructure in solid oxide fuel cells. Electrochimica Acta 2006;52(1):278–84.
[40] Pérez-Flores JC, Ritter C, Pérez-Coll D, Mather GC, García-Alvarado F, Amador U. Synthesis, structures and electrical transport properties of the $La_{2-x}Sr_xNiTiO_{6-\delta}$ ($0 \leq x \leq 0.5$) perovskite series. Journal of Materials Chemistry 2011; 21(35):13195.
[41] Shiratori Y, Tietz F, Buchkremer HP, Stöver D. YSZ-MgO composite electrolyte with adjusted thermal expansion coefficient to other SOFC components. Solid State Ionics 2003;164(1, 2):27–33.
[42] Minh NQ. Ceramic fuel cells. Journal of the American Ceramic Society 1993;76(3):563–88.
[43] Tietz F. Thermal expansion of SOFC materials. Ionics 1999; 5(1):129–39.
[44] Wei B, Lü Z, Jia D, Huang X, Zhang Y, Su W. Thermal expansion and electrochemical properties of Ni-doped $GdBaCo_2O_{5+\delta}$ double-perovskite type oxides. International Journal of Hydrogen Energy 2010;35(8):3775–82.
[45] Zhu X, Le S, Chen X, Sun K, Yuan Y, Zhang N. Chemical compatibility, thermal expansion matches and electrochemical performance of $SrCo_{0.8}Fe_{0.2}O_{3-\delta}$–$La_{0.45}Ce_{0.55}O_{2-\delta}$ composite cathodes for intermediate-temperature solid oxide fuel cells. International Journal of Hydrogen Energy 2011;36(19): 12549–54.
[46] Mitchell RH. Perovskite: Modern and Ancient. Ontario, Canada: Almay Press Inc.; 2002.
[47] Glazer AM. The classification of tilted octahedra in perovskites. Acta Crystallographica Section B 1972;28(11): 3384–92.
[48] Atkinson A, Barnett S, Gorte RJ, Irvine JTS, McEvoy AJ, Mogensen M, et al. Advanced anodes for high-temperature fuel cells. Nature Materials 2004;3(1):17–27.
[49] Lee KT, Manthiram A. $LaSr_3Fe_{3-y}Co_yO_{10-\delta}$ ($0 \leq y \leq 1.5$) intergrowth oxide cathodes for intermediate temperature solid oxide fuel cells. Chemistry of Materials 2006;18(6): 1621–6.
[50] Hjalmarsson P, Søgaard M, Hagen A, Mogensen M. Structural properties and electrochemical performance of strontium- and nickel-substituted lanthanum cobaltite. Solid State Ionics 2008;179(17, 18):636–46.
[51] Zachariasen WH. The crystal structure of monoclinic metaboric acid. Acta Crystallographica 1963;16(5):385–9.

Please cite this article in press as: Pérez-Flores JC, et al., Structural and electrochemical characterization of $La_{2-x}Sr_xNiTiO_{6-\delta}$, International Journal of Hydrogen Energy (2011), doi:10.1016/j.ijhydene.2011.10.101